Force Measurements of the $\alpha_5\beta_1$ Integrin–Fibronectin Interaction

Feiya Li,* Sambra D. Redick,† Harold P. Erickson,† and Vincent T. Moy*
*Department of Physiology and Biophysics, University of Miami School of Medicine, Miami, Florida 33136 and †Department of Cell Biology, Duke University Medical Center, Durham, North Carolina 27710

ABSTRACT The interaction of the $\alpha_5\beta_1$ integrin and its ligand, fibronectin (FN), plays a crucial role in the adhesion of cells to the extracellular matrix. An important intrinsic property of the $\alpha_5\beta_1$/FN interaction is the dynamic response of the complex to a pulling force. We have carried out atomic force microscopy measurements of the interaction between $\alpha_5\beta_1$ and a fibronectin fragment derived from the seventh through tenth type III repeats of FN (i.e., FN7-10) containing both the arg-gly-asp (RGD) sequence and the synergy site. Direct force measurements obtained from an experimental system consisting of an $\alpha_5\beta_1$ expressing K562 cell attached to the atomic force microscopy cantilever and FN7-10 adsorbed on a substrate were used to determine the dynamic response of the $\alpha_5\beta_1$/FN7-10 complex to a pulling force. The experiments were carried out over a three-orders-of-magnitude change in loading rate and under conditions that allowed for detection of individual $\alpha_5\beta_1$/FN7-10 interactions. The dynamic rupture force of the $\alpha_5\beta_1$/FN7-10 complex revealed two regimes of loading: a fast loading regime ($>$10,000 pN/s) and a slow loading regime ($<$10,000 pN/s) that characterize the inner and outer activation barriers of the complex, respectively. Activation by TS2/16 antibody increased both the frequency of adhesion and elevated the rupture force of the $\alpha_5\beta_1$/wild type FN7-10 complex to higher values in the slow loading regime. In experiments carried out with a FN7-10 RGD deleted mutant, the force measurements revealed that both inner and outer activation barriers were suppressed by the mutation. Mutations to the synergy site of FN, however, suppressed only the outer barrier activation of the complex. For both the RGD and synergy deletions, the frequency of adhesion was less than that of the wild type FN7-10, but was increased by integrin activation. The rupture force of these mutants was only slightly less than that of the wild type, and was not increased by activation. These results suggest that integrin activation involved a cooperative interaction with both the RGD and synergy sites.

INTRODUCTION

The interaction between $\alpha_5\beta_1$ integrin and fibronectin (FN) plays an important role in cell differentiation, proliferation (Garcia et al., 1999; Molla and Block 2000) and migration (Pierini et al., 2000) by serving as a bridge between the cell and the extracellular matrix that mediates bidirectional signaling events through inside-out and outside-in pathways (Yamada and Miyamoto 1995; Fernandez et al., 1998). Altered expression of the $\alpha_5\beta_1$ integrin and fibronectin has been correlated with both physiological and pathological processes including neural development, wound healing, tumor metastasis, and atherosclerosis (Barillari et al., 2001; Greiling and Clark, 1997; Taverna and Hynes, 2001; Goh et al., 1997). In animal models, mouse embryos lacking fibronectin showed defects in the mesoderm, the neural tube, and in vascular development, and died by embryonic day 9 (George et al., 1993).

Submitted July 16, 2002, and accepted for publication September 30, 2002.

Address reprint requests to Vincent T. Moy, Dept. of Physiology and Biophysics, University of Miami School of Medicine, 1600 N.W. 10th Avenue, Miami, FL 33136. Tel.: 305-243-3201; Fax: 305-243-5931; E-mail: vmoy@newssun.med.miami.edu.

Abbreviations used: fibronectin, FN; atomic force microscopy, AFM; arginine-glycine-asparate, RGD; proline-histidine-serine-arginine-asparagine PHSRN; high affinity $\alpha_5\beta_1$, h$\alpha_5\beta_1$; low affinity $\alpha_5\beta_1$, l$\alpha_5\beta_1$; leukocyte function-associated antigen-1, LFA-1; intercellular adhesion molecule-1, ICAM-1; FN7-10(R1374A/P1376A/R1379A), FN7-10(Δsyn); FN7-10 with RGDS deleted, FN7-10(ΔRGD).

0006-3495/03/02/1252/11 $2.00

The integrin $\alpha_5\beta_1$ is one of 24 known members of the integrin family of adhesion molecules, formed by the noncovalent assembly of an α-subunit (i.e., α_5) and a β-subunit (i.e., β_1) (Hynes, 1992). Both subunits consist of large extracellular domains of more than 940 (α_5) and 630 residues (β_1), a transmembrane domain, and a short cytoplasmic domain (Coe et al., 2001; Mould et al., 1997). The current model for the structural organization of $\alpha_5\beta_1$ is largely based on the crystal structure of the $\alpha_V\beta_3$ integrin (Xiong et al., 2001). The ligand-binding ''head'' region of the $\alpha_5\beta_1$ is formed by the N-terminal seven bladed β-propeller domain of α_5 and the I-like domain of β_1 (Mould et al., 2000; Springer 1997). Structural elements in the ''head'' region implicated in FN binding include the metal ion dependent adhesion site (MIDAS) of β_1, and the two to four repeats of the β-propeller of α_5 (Coe et al., 2001; Xiong et al., 2001; 2002).

Fibronectin, a major element of the extracellular matrix in many tissues, is a dimeric glycoprotein, and serves as a ligand for $\alpha_5\beta_1$. Each subunit is composed of multiple homologous domains termed FNI, FNII, and FNIII. The arg-gly-asp (RGD) sequence in FNIII domain 10 (FN10) is the crucial attachment site for FN receptors, including the integrin $\alpha_5\beta_1$ (Pierschbacher and Ruoslahti, 1984; Yamada and Kennedy, 1984). A synergy site that is important for binding $\alpha_5\beta_1$ is located in FN9 (Aota et al., 1994; Kimizuka et al., 1991; Obara et al., 1988, Danen et al., 1995). The sequence PHSRN was earlier reported to be important for the synergy effect (Bowditch et al., 1994, Aota et al., 1994) but more recently the synergy site has been identified as a more extended surface of FN9 (Redick et al., 2000; Kauf et al., 2001).

In recent years extensive studies have been focused on the molecular basis of integrin–ligand binding. The binding pocket of the $\alpha_5\beta_1$/fibronectin interaction appears to be more complex and involves both α- and β-subunits of the integrin and FN9 and FN10 of fibronectin as determined by antibody mapping, mutagenesis, and structural studies. Crystallographic analysis of the $\alpha_V\beta_3$ integrin complexed to a cyclic RGD peptide suggests that the RGD loop in FN10 is recognized by both α_5 and β_1 subunits (Xiong et al., 2002). The aspartate residue coordinates with the metal ion in the MIDAS of the βA domain and the arginine and glycine residues make contact with the β-propeller of the α_5 subunit (Xiong et al., 2002). The synergy site in FN9 comprises half a dozen surface amino acids on the side of the domain facing the direction of the RGD (Redick et al., 2000, Kauf et al., 2001) and is recognized primarily by the third and fourth repeats in the β-propeller of the α_5 subunit (Burrows et al., 1999; Mould et al., 1997; Mould et al., 1998).

Recent models predict that the $\alpha_5\beta_1$ integrin can exist in multiple conformational states (inactivated, intermediate activated, and fully activated) that have different affinities for FN (Garcia et al., 1998b). The $\alpha_5\beta_1$ integrin is activated by inside-out signaling that appears to act on the cytoplasmic tails, which releases the constraint between the two subunits and subsequently exposes a high affinity ''open'' conformation for ligand binding (Takagi et al., 2001). $\alpha_5\beta_1$ can also be activated by nonphysiological stimuli such as activating monoclonal antibodies (e.g., TS2/16 and AG89; Arroyo et al., 1993; Tsuchida et al., 1998) and high concentrations of extracellular Mg^{2+} or Mn^{2+} (Mould et al., 1995). Structural analysis of the $\alpha_V\beta_3$ integrin has lent support to the idea that $\alpha_5\beta_1$ activation may involve conformational change in the βA domain and a reorientation of the extracellular domains of the α- and β-subunits (Xiong et al., 2002).

Cell–matrix interactions usually occur in the context of a complex process where either an external or internal force acts on the cell. For example, when cells migrate, the traction force generated inside the cell is applied to the integrin/FN linkages. It is, therefore, important to understand how a pulling force affects the dynamics of the integrin–ligand complex.

A number of advanced techniques have been developed to measure the rupture force of molecular adhesion. Commonly used techniques employed in single molecule force measurements include the biomembrane force probe (Evans et al., 1995), the atomic force microscopy (AFM) (Moy et al., 1994), optical tweezers (Litvinov et al., 2002; Thoumine et al., 2000; Thoumine and Meister, 2000), and the parallel-plate flow chamber (Chen and Springer 2001). The dynamics of selectin-mediated adhesion was characterized by biomembrane force probe and AFM measurements (Evans et al., 2001; Fritz et al., 1998), and in the parallel-plate flow chamber (Chen and Springer 2001). The AFM technique was also used to measure the adhesion force between osteoblast and several RGD-containing ligands (Lehenkari and Horton 1999). In a recent study closely related to ours, Litvinov et al. (2002) used laser tweezers to measure the rupture force of $\alpha_{IIb}\beta_3$ integrin to fibrinogen, with the integrin both on living platelets and as purified protein (Litvinov et al., 2002).

In this report, we present direct force measurements, acquired by AFM, of the interaction between the integrin $\alpha_5\beta_1$ and fibronectin. In these experiments, we used the K562 cell line, which expresses the $\alpha_5\beta_1$ integrin, but no other FN receptors (Hemler et al., 1987). Our measurements were carried out using the fibronectin fragment, FN7-10, which consists of FN type III repeats 7–10, rather than whole plasma fibronectin to avoid misinterpretation of measurements acquired from a system that has multiple binding sites (Hocking et al., 1998). The $\alpha_5\beta_1$ integrins of K562 cells are constitutively inactive, but can be activated by various monoclonal antibodies against β_1 (e.g., TS2/16). The acquired data were analyzed in the framework of the dynamic force model of Evans and Ritchie (1997). Studies were also carried out with FN fragments that contain either a deletion of RGD sequence or mutations of the synergy site to identify the contributions of these sites to the interactions of the $\alpha_5\beta_1$/FN complex.

METHODS

Cells and reagents

The $\alpha_5\beta_1$-expressing K562 (ATCC, CCL-243) cell lines was maintained in continuous culture in RPMI 1640 medium supplemented with 10% heat-inactivated fetal calf serum (Irvine Scientific, Santa Ana, CA), penicillin (50 U/ml, Gibco BRL, Grand Island, NY) and streptomycin (50 μg/ml, GIBCO BRL). The K562 cells were expanded on a 3-day cycle.

The TS2/16 monoclonal antibody, which activates β_1 integrins, was derived from supernatants of hybridoma cells (ATCC, HB243) maintained in culture. The K562 cells were activated by adding 1/10 volume (v/v) of TS2/16 culture supernatant for 10 min at room temperature. The anti-β_1 integrin monoclonal antibody, P5D2, which inhibits the binding of β_1 integrins to FN, was a generous gift from Dr. J. Li (Dept. of Dermatology, University of Miami) (Caixia et al., 1991). JBS5 is a mouse IgG against α_5 integrins and was purchased from Serotec (Raleigh, NC) (Wayner et al., 1993). Polyclonal mouse IgG was purchased from Sigma (St. Louis, MO).

A plasmid containing FN7-10 in the pET11b vector was previously described (Aukhil et al., 1993; Leahy et al., 1996). A mutant deleting the RGD (FN7-10(ΔRGDS)), and a triple mutant that inactivates the synergy site (FN7-10(R1374A/P1376A/R1379A), referred to as FN7-10(Δsyn)), were described in Redick et al. (2000). Proteins were expressed in BL21 cells and purified by $(NH_4)_2SO_4$ precipitation followed by chromatography on a mono Q and crystallization in low pH sodium formate (Redick et al., 2000). Human plasma fibronectin (pFN) was purchased from Sigma and used without further purification.

Attachment of cell to AFM cantilever

K562 cells were attached to the AFM cantilever by concanavalin A (Con A)-mediated linkages. The cantilevers were soaked in acetone for 5 min, UV irradiated for 30 min, and incubated in biotinamidocaproyl-labeled bovine serum albumin (biotin-BSA, 0.5 mg/ml; Sigma) overnight at 37°C. The cantilevers were then rinsed three times with phosphate buffer and incubated in 0.5 mg/ml streptavidin (Pierce; Rockford, IL) for 10 min at room temperature. After the removal of unbound streptavidin, the cantilevers were

incubated in 0.5 mg/ml biotinylated Con A (Sigma) and then rinsed. To attach the cell to the cantilever, the tip of the Con A-functionalized cantilever was positioned above the cell and lowered onto the cell for ~1 s. The attached cell was positioned behind the tip of the cantilever as shown in Fig. 1. To obtain an estimate of the strength of the cell–cantilever linkage, we allowed the attached cell to interact with a petri dish coated with Con A. Upon retraction of the cantilever, separation always ($N > 20$) occurred between the cell and the Con A-coated petri dish. In these measurements, the average force needed to induce separation was >2 nN, much larger than the forces found for an individual $\alpha_5\beta_1$/FN bond. This observation is important inasmuch as it ensures that the cell remained bound to the cantilever during the single molecule $\alpha_5\beta_1$/FN force measurements.

Immobilized protein

Whole human plasma fibronectin, FN7-10, or FN7-10 with deleted RGD or synergy site mutants (100 μg/ml in 0.1M $NaHCO_3$) were adsorbed overnight at 4°C on 35-mm tissue culture dishes. Unbound FNs were removed and the dish was incubated with 1% bovine albumin for 1 h at 37°C to block the exposed surface of the tissue culture dish.

AFM force measurements

The AFM force measurements were performed on an apparatus designed to be operated in the force spectroscopy mode (Heinz and Hoh, 1999). A K562 cell was attached to the end of the AFM cantilever as described above. A piezoelectric translator was used to lower the cantilever/cell onto the FN-coated dish. Contact between the attached K562 cell and the sample was indicated by deflection of the cantilever, which was measured by reflecting a laser beam off the cantilever into a position sensitive two-segment photodiode detector.

Measurements of unitary $\alpha_5\beta_1$/FN rupture forces were obtained under conditions that minimized contact between the K562 cell and the FN-coated dish. An adhesion frequency of <30% in the force measurements ensured that there is a >83% probability that the adhesion event is mediated by a single $\alpha_5\beta_1$/FN bond (Merkel et al., 1999; Tees et al., 2001). We were able to acquire measurements with loading rates between 10 and 50,000 pN/s by adjusting the retraction speed of the cantilever (1–15 μm/s) and by variations in the local elasticity of the cell (0.01–5.0 mN/m) that allowed for the system spring constant (the cell–cantilever combination) to vary between 0.01 and 3.33 mN/m. To satisfy the condition of constant loading rate required for our analysis, measurements were selected for our analysis only if there was a sustained linear increase in force with respect to time before bond dissociation. At fast cantilever retraction speeds (>1 μm/s), the hydrodynamic drag on the cantilever resulted in smaller forces recorded than were actually applied to rupture the complex. To correct for the hydrodynamic force exerted on the cantilever, we determined the damping coefficient of the cantilever ξ (~2 pN-s/μm) in the culture medium by measuring the deflection of cantilever at different retraction speeds. The rupture force plotted in Figs. 4–8 is the sum of the measured force and the hydrodynamic force. All AFM force measurements were carried out at 25°C with fresh culture medium supplemented with 10 mM HEPES buffer.

The AFM cantilevers were purchased from TM Microscopes (Sunnyvale, CA). The largest triangular cantilever (320 μm long and 22 μm wide) from a set of five on the cantilever chip was used in our measurements. These cantilevers were calibrated by analysis of their thermally induced fluctuation to determine their spring constant (Hutter and Bechhoefer, 1993). The experimentally determined spring constants were consistent with the nominal value of 10 mN/m given by the manufacturer.

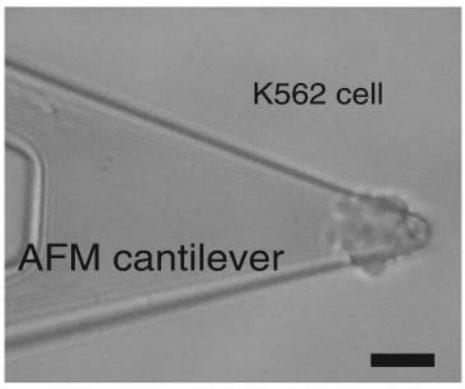

FIGURE 1 Micrograph of a K562 cell attached to the end of an AFM cantilever. The bar is 20 μm.

RESULTS

Measurements of $\alpha_5\beta_1$/FN interactions by AFM

Direct force measurements by AFM were employed to characterize the adhesive interaction between immobilized FN and $\alpha_5\beta_1$ integrin expressed on the surface of the human chronic myelogenous leukemia cell line, K562. The cell adhesion studies were carried out with a K562 cell coupled to the AFM cantilever and FN adsorbed to a tissue culture dish (Fig. 1). In these measurements, the K562 cell was lowered onto the dish until contact was made. The interaction between the cell and the dish was regulated by the applied force of 100–500 pN exerted by the cantilever. After a given contact duration, the K562 cell was withdrawn from the dish at a separation rate of 5 μm/s while the force versus piezo displacement trace of the process was recorded (Fig. 2 A). The adhesive interactions between the cell and protein coating on the dish were detected as downward deflections of the cantilever. We and others have found that this experimental design allows investigators to study the dynamics of cell adhesion involving many adhesion molecules, as well as the properties of individual molecular complexes (Benoit et al., 2000; Zhang et al., 2002).

Fig. 2 *A* presents measurements acquired under conditions where cell adhesion was mediated by multiple $\alpha_5\beta_1$/FN7-10 complexes. These complexes did not necessarily rupture simultaneously during detachment as revealed by the ''sawtooth'' profile in the AFM traces. Each of the force jumps as indicated by the arrows in Fig. 2 *A* is interpreted to correspond to the breakage of one or more $\alpha_5\beta_1$/FN7-10 complexes. It is unlikely that these force jumps corresponded to the breakage of other molecular linkages and/or the unfolding of proteins on the basis of single molecule measurement analysis as discussed below. Adhesion between the K562 cell and FN7-10 increased after the addition of TS2/16, an activating monoclonal antibody against β_1 integrins (Arroyo et al., 1993). Activation of $\alpha_5\beta_1$ by TS2/16 was dose-dependent. 10% culture supernatant of TS2/16 (~1 μg/ml antibody in final concentration) was sufficient to fully activate $\alpha_5\beta_1$. Higher concentrations (up to 20 μg/ml)

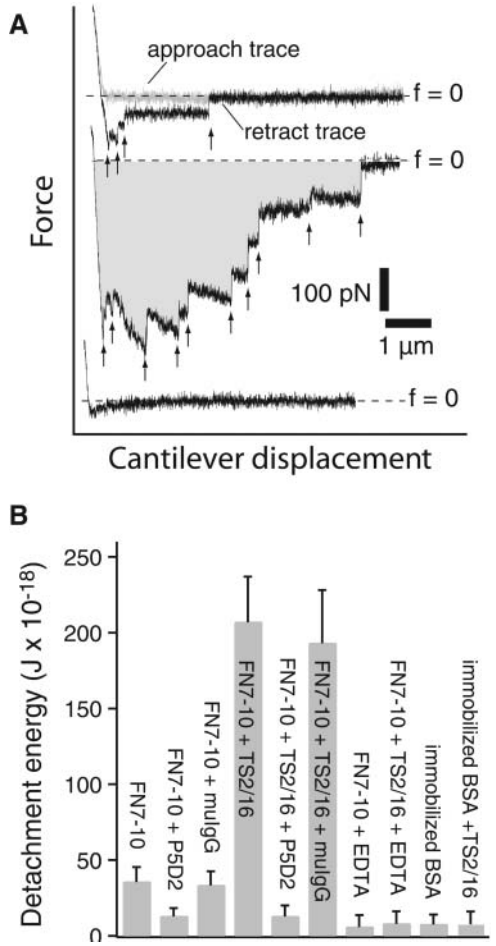

FIGURE 2 AFM force measurements of $\alpha_5\beta_1$-mediated cell adhesion. (*A*) A series of AFM force-displacement retract traces of the interaction between an unactivated K562 cell and FN7-10 (*top record, approach and retract traces*), after the K562 cell was activated by 10% TS2/16 (*middle record, retract trace only*) and in the presence of antibodies (P5D2, 20 μg/ml) against the β-subunit of $\alpha_5\beta_1$ (*bottom record, retract trace only*). The arrows point to the positions in the traces where the $\alpha_5\beta_1$/FN7-10 complex ruptured. The shaded area in the middle trace is the detachment energy. (*B*) Detachment energies of $\alpha_5\beta_1$-mediated cell adhesion for different cell states. Higher detachment energies are due to both a larger number of adhesions and larger forces of detachment. The error bar is the standard deviation.

of TS2/16 did not augment adhesion relative to the adhesion level observed with 1 μg/ml TS2/16 (data not shown). As shown in the middle trace of Fig. 2 *A*, the number of force jumps increased, reflecting the increase in the number of $\alpha_5\beta_1$/FN7-10 complexes formed after TS2/16 treatment. The addition of P5D2, a function-blocking anti-β_1 monoclonal antibody significantly lowered the adhesion (Fig. 2 *A*, *bottom trace*), whereas antimouse IgG (50 μg/ml) had no effect on cell adhesion.

Fig. 2 *B* summarizes the results from a series of force measurements using the detachment energy to quantify cell adhesion under different experimental conditions. The detachment energy was obtained by integrating the pulling force over displacement of the cell until the last of the $\alpha_5\beta_1$/FN complexes ruptured. It should be noted that this detachment energy is the work done to break the $\alpha_5\beta_1$ bonds as well as the work done to deform the cell during the detachment process. The detachment energy depends on the number of $\alpha_5\beta_1$/FN complexes formed when the cell is pressed against the FN-coated substrate, and hence on the applied force and the duration of cell–substrate contact. To permit direct comparison of the detachment energy, the values plotted in Fig. 2 *B* were obtained from measurements carried out at the same compression force (150 pN), contact duration (1 s), and retraction speed (5 μm/s). As shown, adhesion was augmented fivefold by integrin activation with the TS2/16 antibody. Adhesions of both untreated and activated cells to FN7-10 were inhibited by the anti-β_1 antibody, P5D2 (20 μg/ml), and by 5 mM EDTA, but not by nonspecific polyclonal murine IgG (50 μg/ml). Moreover, both untreated and activated cells did not adhere to immobilized BSA. These experiments demonstrated that the adhesion between K562 and an FN-coated petri dish was largely due to the $\alpha_5\beta_1$/FN interaction.

AFM measurements of individual $\alpha_5\beta_1$/FN interactions

To assess the bond strength of an individual $\alpha_5\beta_1$/FN7-10 interaction, contact between the cell and the dish was minimized by reducing both contact duration (<50 ms) and compression force (100 pN). Examples of unfiltered force measurements acquired under these conditions are shown in Fig. 3 *A*. Under these conditions ~30% of measurements resulted in adhesion (i.e., a 30% frequency of adhesion). Traces that registered a sharp transition of more than 30 pN were counted as an adhesion event. Forces of less than 30 pN were excluded inasmuch as the observed fluctuations of the free cantilever were frequently 20 pN. The rupture force of the $\alpha_5\beta_1$/FN7-10 complex was derived from the magnitude of the force transition after correction for hydrodynamic drag. It should be noted that the majority of the measurements acquired under these conditions registered a single transition in force. This transition stemmed from the forced unbinding of a single $\alpha_5\beta_1$/FN7-10 complex. Moreover, such observations also revealed that the dissociation of the $\alpha_5\beta_1$/FN7-10 complex does not involve the initial unfolding of the proteins as observed in the forced unfolding of FN domains (Oberhauser et al., 1998).

To assess the contributions of the RGD loop and of the synergy site residues of FN to the binding force of the $\alpha_5\beta_1$/FN interaction, we have obtained measurements of the mean rupture forces of untreated and activated $\alpha_5\beta_1$ complexed to FN7-10, FN7-10(Δsyn), and FN7-10(ΔRGD). The force values presented in Fig. 3 *B* were from measurements acquired at loading rates of 1800–2000 pN/s. Under these conditions, the mean rupture force of the $\alpha_5\beta_1$/FN7-10 complex was elevated from 69 pN ± 1.5 (mean ± SE) to 93 pN ± 1.5 after integrin activation by the TS2/16 mAb.

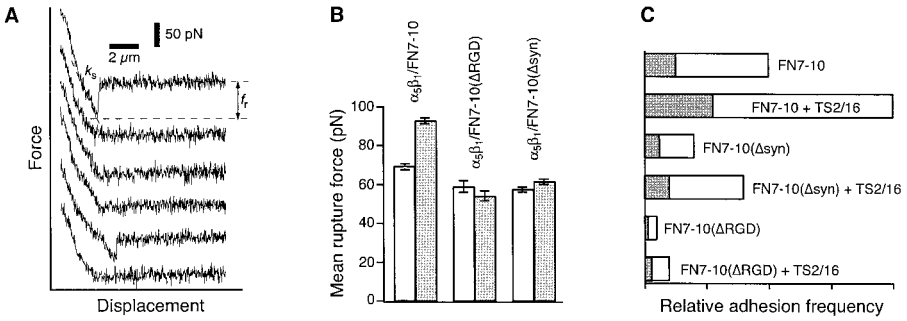

FIGURE 3 (*A*) Force-displacement traces between K562 and FN7-10 under conditions of minimal contact. Two of the six traces (first and fifth) revealed adhesion. f_r is the rupture force of the $\alpha_5\beta_1$ integrin/FN bond. k_s is the system spring constant and is used to determine the loading rate of the measurement. The cantilever retraction rate of the measurements was 5 μm/s. (*B*) Mean rupture forces of individual $\alpha_5\beta_1$ integrins complexed to FN7-10, FN7-10 (ΔRGD), and FN7-10(Δsyn). Measurements were acquired at a loading rate of 1,800 pN/s. Open and gray bars correspond to measurements from untreated and TS2/16 activated cells, respectively. The error bar is the standard error of the mean. (*C*) Adhesion frequency of K562/FN binding under conditions of limited tip–substrate contact. Open and gray bars correspond to adhesion frequencies before and after the addition of the function-blocking antibody, JBS5 (20 μg/ml), respectively.

However, there was no enhancement in the bond strength of either $\alpha_5\beta_1$/FN7-10(Δsyn) or $\alpha_5\beta_1$/FN7-10(ΔRGD) complexes after antibody activation. The force measurements also revealed a slightly lower rupture force for both $\alpha_5\beta_1$/FN7-10(Δsyn) and $\alpha_5\beta_1$/FN7-10(ΔRGD) complexes relative to the wild type complex.

The specificity of these measurements was verified by a significant reduction in the frequency of adhesion after the addition of the function-blocking anti-α_5 antibody, JBS5 (Fig. 3 *C*). The frequency of adhesion did not change when polyclonal murine IgG (50 μg/ml) was added (data not shown). Interestingly, the frequency of adhesion for $\alpha_5\beta_1$/FN7-10 interactions is only doubled when the integrin is activated. However, it should be emphasized that the adhesion frequency is dependent on the association rate of the $\alpha_5\beta_1$/FN interaction and the lateral diffusion of $\alpha_5\beta_1$. Inasmuch as the force measurements were carried out with surface contact time of less than 50 ms, there was insufficient time for a complete lateral redistribution of membrane proteins. Hence, under these conditions, differences in the frequency of adhesion of the different $\alpha_5\beta_1$/FN pairs reflected differences in the association rate (k_{on}) of the different pairs. Our observation that the number of adhesions is only doubled for FN7-10 when the integrin is activated revealed that the k_{on} of activated $\alpha_5\beta_1$ is slightly faster than the k_{on} of the low affinity $\alpha_5\beta_1$. This suggests that the enhanced cell adhesion stemmed primarily from changes in the dissociation rate of the complex.

Fig. 4, *A–D* present histograms of the rupture force of the $\alpha_5\beta_1$/FN7-10 complex. A shift in the force histogram toward higher forces was observed with increasing force loading rates for both untreated (compare Fig. 4, *A* and *B*) and TS2/16 activated (compare Fig. 4, *C* and *D*) K562 cells. There was also a shift toward higher forces (compare Fig. 4, *A* and *C*) upon cell activation at a slow loading rate (230–240 pN/s), but not at the fast loading rate of 13,000–13,500 pN/s (compare Fig. 4, *B* and *D*). Fig. 4 *E* presents the force spectrum (i.e., force versus loading rate relation) of the $\alpha_5\beta_1$/FN7-10 interaction for loading rates of 20 pN/s to 50,000 pN/s. The force spectrum revealed that the rupture force of the $\alpha_5\beta_1$/FN7-10 complex increased gradually over three orders of magnitude in loading rate. After $\alpha_5\beta_1$ activation with the TS2/16 antibody, the rupture forces of the complex were elevated over the range of loading rates between 20 to 10,000 pN/s, but did not change the dynamic response of the

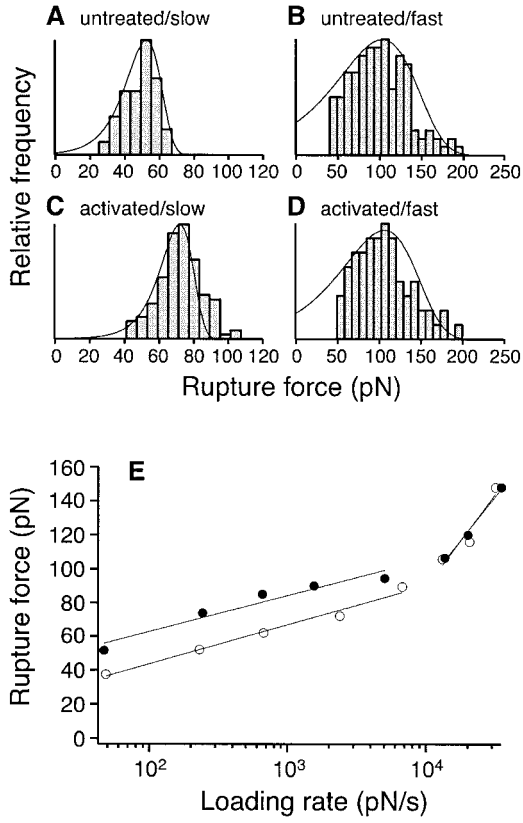

FIGURE 4 Measurements of the rupture force of individual $\alpha_5\beta_1$ integrin/fibronectin bonds at different loading rates. (*A, B*) Force histograms of $\alpha_5\beta_1$/FN7-10 interaction at (*A*) slow (230 pN/s) and (*B*) fast (13,000 pN/s) loading rates. (*C, D*) Force histograms of the high affinity $\alpha_5\beta_1$/FN7-10 interaction (activated by TS2/16) at (*C*) slow (240 pN/s) and (*D*) fast (13,500 pN/s) loading rates. The fitted probability density functions (Eq. 1) in *A–D* were obtained using the Bell model parameters listed in Table 1. (*E*) Single molecule force measurements between FN7-10 and unactivated K562 cells (*open circle*) or 10% TS2/16 activated K562 cells (*solid circle*) as a function of loading rates. The best-fit curves (*gray lines*) were obtained using Eq. 2 (see Discussion).

TABLE 1 Bell model parameters of the $\alpha_5\beta_1$/fibronectin interaction

$\alpha_5\beta_1$/FN pair	Loading rate (pN/s)	k° (s−1)	γ (Å)
l$\alpha_5\beta_1$/FN7-10	20–10,000	0.13	4.1
	10,000–50,000	33.5	0.86
h$\alpha_5\beta_1$/FN7-10	20–10,000	0.012	4.4
	10,000–50,000	29.1	0.91
l$\alpha_5\beta_1$/FN7-10(ΔRGD)	20–50,000	0.13	4.6
h$\alpha_5\beta_1$/FN7-10(ΔRGD)	20–50,000	0.19	4.1
l$\alpha_5\beta_1$/FN7-10(Δsyn)	20–10,000	0.85	3.65
	10,000–50,000	25.0	0.95
h$\alpha_5\beta_1$/FN7-10(Δsyn)	20–10,000	0.66	3.27
	10,000–50,000	24.9	0.91

complex at loading rates greater than 10,000 pN/s. Similar results were obtained in force measurements between K562 cells and plasma fibronectin immobilized on a solid surface (Fig. 5).

In our AFM measurements, it was assumed that the measured rupture force stemmed from the unbinding of the $\alpha_5\beta_1$/FN complex, although there are other linkages that can break during the measurement. For example, it is conceivable that $\alpha_5\beta_1$ could be extracted from the cell membrane or that FN could come unbound from the surface of the petri dish. However, inasmuch as the interaction of $\alpha_5\beta_1$ with plasma FN and FN7-10 displayed similar force spectra (Fig. 5), it is unlikely that the measured rupture force stemmed from the detachment of FN. An earlier study (Garcia et al., 1998a), using fluid shear to detach cells, showed that when the $\alpha_5\beta_1$/FN bond was stabilized by covalent cross-linking, the force for detachment doubled. This implies that this bond is weaker than that holding the integrin in the membrane, or attaching FN to the substrate. Nevertheless, to demonstrate that $\alpha_5\beta_1$ remained anchored to the cell membrane, we fixed K562 cells by brief exposure to a 1% glutaraldehyde solution. As shown in Fig. 6, the force spectrum of the $\alpha_5\beta_1$/FN complex obtained using the fixed cells is similar to

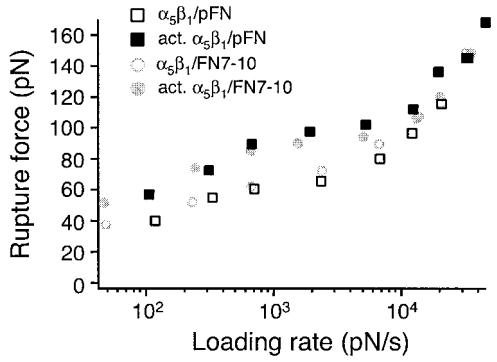

FIGURE 5 Single molecule force measurements between human plasma fibronectin and unactivated K562 cells (*open square*) or K562 cells (*solid square*) activated by TS2/16. The mode rupture force is plotted as a function of loading rates. Measurements of the $\alpha_5\beta_1$/FN7-10 interaction are plotted in open and closed circles.

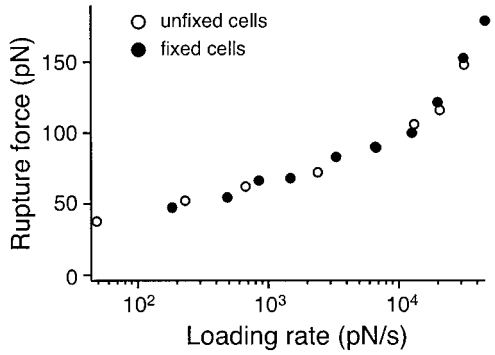

FIGURE 6 Single molecule force measurements of the interactions between live K562 (*open circle*) or fixed K562 cells (*solid circle*) and FN7-10. The mode rupture force is plotted as a function of loading rates.

the force spectrum obtained using live cells, an observation that is consistent with $\alpha_5\beta_1$ remaining attached to the cell. Considered together, these observations are all consistent with the measured breakage occurring at the $\alpha_5\beta_1$/FN junction. Moreover, the measurements acquired with the fixed cells also served to demonstrate that the viscoelastic properties of the K562 cell did not significantly alter the force measurements.

Deletion of the RGD loop from FN7-10 suppressed the rupture force at fast loading rates

To assess the role of the RGD loop of FN10 in the interactions of $\alpha_5\beta_1$ with FN, we have also carried out AFM measurements between individual $\alpha_5\beta_1$ integrin and a fibronectin fragment with the RGD loop deleted. Although the interaction between $\alpha_5\beta_1$ and FN7-10(ΔRGD) was weak, we were able to demonstrate specific binding by measuring the adhesion frequency before and after the addition of the inhibitory anti-α_5 monoclonal antibody JBS5. Under conditions that resulted in an initial 10% adhesion frequency, the addition of the JBS5 lowered the adhesion frequency to <3%, a 70% reduction (Fig. 3 *C*). The addition of polyclonal murine IgG (50 μg/ml) did not affect adhesion (data not shown).

Fig. 7 presents the force spectra of the interaction between the FN7-10 RGD deletion mutant and $\alpha_5\beta_1$ of untreated and TS2/16 activated K562 cells. There were two striking differences between FN7-10(ΔRGD) and wild type FN7-10. First, the TS2/16 antibody showed no elevation of the rupture force. The force at lower loading rates was comparable to that for FN7-10, but there was no increase upon activation. Second, the binding to FN7-10(ΔRGD) did not show the increase in slope at high loading rates. Thus, it appears that the inner activation barrier of the $\alpha_5\beta_1$/FN interaction was suppressed by the deletion of the RGD sequence from FN.

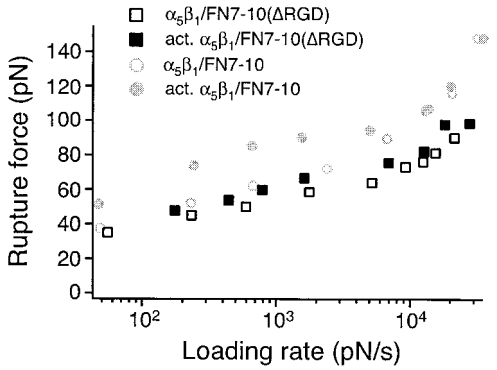

FIGURE 7 Measurements of the rupture force between individual FN7-10 (ΔRGDS) and $\alpha_5\beta_1$ integrin in unactivated K562 (*open square*) or activated K562 cells (*solid square*). The mode rupture force is plotted as a function of loading rates. The data plotted in gray circles are measurements between FN7-10 and unactivated K562 (*open circle*) or activated K562 cells (*solid circle*).

Mutations to the synergy site of fibronectin suppressed the rupture force at slow loading rates

The binding of FN to $\alpha_5\beta_1$ is significantly enhanced by interactions of the synergy site residues within FN9 with $\alpha_5\beta_1$ (Aota et al., 1994; Kimizuka et al., 1991; Obara et al., 1988; Redick et al., 2000; Kauf et al., 2001). To assess the contribution of the synergy site residues in the $\alpha_5\beta_1$/FN interaction, we have carried out AFM force measurements with a FN fragment with triple mutations in the synergy site (R1374A/P1376A/R1379A) (Fig. 8). The interaction between $\alpha_5\beta_1$ and FN7-10(Δsyn), the synergy site mutant, was weak, but detectable. As with the RGD deletion mutant, the binding to FN7-10(Δsyn) was not enhanced when the integrin was activated by TS2/16. However, in contrast to the RGD mutant, binding to FN7-10(Δsyn) showed the increased force slope at high loading rates, essentially the same as wild type FN7-10.

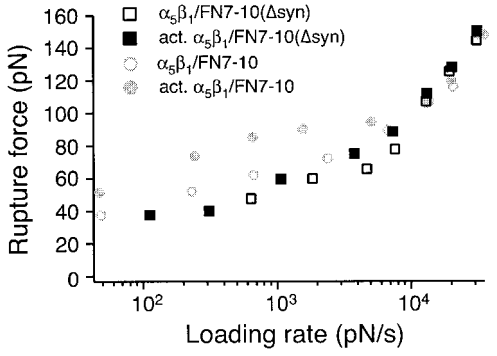

FIGURE 8 Measurements of the rupture force between individual FN7-10(Δsyn) and unactivated K562 (*open square*) or activated K562 (*solid square*) cells. The mode rupture force is plotted as a function of loading rates. The data plotted in gray circles are measurements between FN7-10 and unactivated K562 (*open circle*) or activated K562 cells (*solid circle*).

DISCUSSION AND CONCLUSIONS

A theoretical framework for understanding how force can affect the adhesion complex was proposed by Bell (Bell et al., 1984), and later expanded on by other researchers (Evans and Ritchie, 1997; Merkel et al., 1999). In this model, an applied force f distorts the energy landscape of the $\alpha_5\beta_1$/FN complex resulting in a lowering of the activation barrier(s), and consequently increases the dissociation rate constant $k(f)$ as follows: $k(f) = k^\circ \exp[f\gamma/k_BT]$ where k° is the dissociation rate constant in the absence of the applied force, γ is the position of the transition state, T is temperature, and k_B is Boltzmann's constant. Under conditions of constant loading r_f, the probability density function for the forced unbinding of the adhesion complex is given by:

$$P(f) = k^\circ \exp\left(\frac{\gamma f}{k_B T}\right)\exp\left\{\frac{k^\circ k_B T}{\gamma r_f}\left(1 - \exp\left(\frac{\gamma f}{k_B T}\right)\right)\right\}. \quad (1)$$

Moreover, the mode of the rupture force distribution f_m can be expressed as a linear function of the $\ln(r_f)$,

$$f_m = \frac{k_B T}{\gamma}\ln\left(\frac{\gamma}{k^\circ k_B T}\right) + \frac{k_B T}{\gamma}\ln(r_f), \quad (2)$$

where the y-intercept is

$$y_o = \frac{k_B T}{\gamma}\ln\left(\frac{\gamma}{k^\circ k_B T}\right)$$

and the slope

$$m = \frac{k_B T}{\gamma}.$$

(see Tees et al., 2001). The force-induced dissociation of a ligand–receptor complex may involve overcoming multiple activation energy barriers. In the case where the system must overcome a series of increasingly higher activation barriers before final dissociation, the dissociation kinetics of the complex at low pulling forces is governed by the properties of the outermost barrier. With increasing pulling forces the outermost barriers are suppressed and the dissociation kinetics of the system is then governed by the properties of an inner activation barrier. Similarly, the force spectrum of the system is divided into multiple loading regimes that characterize the individual activation energy barriers. The dynamic strength (i.e., rupture forces) of the complex measured in slow loading regimes characterizes the outermost activation energy barriers, whereas the force measurements obtained in the fast loading regimes characterize the innermost barriers (Evans and Ritchie, 1997).

An examination of the force spectra of the $\alpha_5\beta_1$/FN7-10 interaction revealed that our measurements of the $\alpha_5\beta_1$/FN7-10 interaction are not compatible with the single barrier Bell model. However the acquired force spectra is consistent with

an intermolecular potential that consisted of two activation energy barriers. These energy barriers were characterized by fitting Eq. 2 to the acquired force measurements. The fitted curves are overlaid on the measurements in Fig. 4 *E* and the best-fit parameters, k° and γ, are tabulated in Table 1. In Table 1, l$\alpha_5\beta_1$ and h$\alpha_5\beta_1$ correspond to the low and high affinity form of $\alpha_5\beta_1$, respectively. This analysis revealed that the forced unbinding of $\alpha_5\beta_1$/FN7-10 complex involved overcoming at least two activation barriers. The positions of the transition states of the inner and outer barriers from equilibrium are ~0.9 Å and ~4.2 Å, respectively, for both the low and high affinity forms of the $\alpha_5\beta_1$/FN7-10 complex. Moreover, our analysis revealed that the observed increase in rupture force after integrin activation in the low loading regime stemmed from an elevation of the outer activation energy barrier, which is manifested in a lowering of the dissociation rate constant from 0.13/s to 0.012/s. These values are consistent with the dissociation rates obtained in other studies (Akiyama and Yamada, 1985; Thoumine et al., 2000). The inner activation barrier appeared unaffected by the integrin activation via TS2/16 inasmuch as there was no change in the dynamic strength of the complex in the fast loading regime after activation. To determine more precisely the change in activation energy of the complex after TS2/16 binding, we estimated that the energy differences ($\Delta\Delta G^{\dagger}$) between transition state energies of high and low affinity complexes ($\Delta G_H^{\dagger}$) and ($\Delta G_L^{\dagger}$) to be ~0.14 k_BT for the inner barrier and ~2.38 k_BT for the outer barrier (see Fig. 9). From this analysis, we concluded the high affinity state of the $\alpha_5\beta_1$/FN7-10 complex stemmed from the elevation of the outer activation energy barrier of the complex.

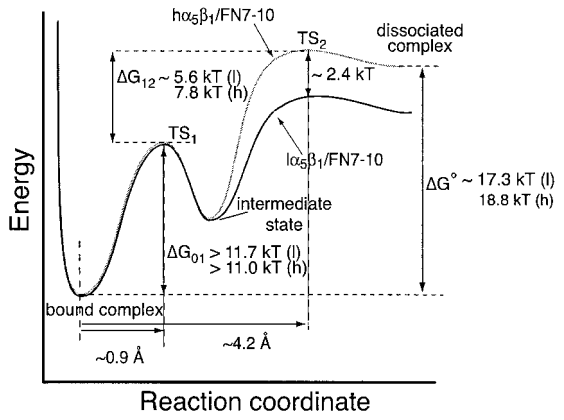

FIGURE 9 Intermolecular potential of the $\alpha_5\beta_1$/FN7-10 interaction. The forced dissociation of the $\alpha_5\beta_1$/FN7-10 involves overcoming two transition states, TS_1 and TS_2. Estimates of the equilibrium free energies (ΔG^{O}) were derived from the equilibrium affinity constants reported in Takagi et al. (2001). (*l*) and (*h*) denote energies corresponding to the low and high affinity $\alpha_5\beta_1$/FN7-10 complexes, respectively. Estimates of the energy difference (ΔG_{12}) between TS_1 and TS_2 were obtained using: $\Delta G_{12} = -k_BT\ln(k_1^{\circ}/k_2^{\circ})$ where k_1° and k_2° are the dissociation rate constants of the inner and outer activation energy barriers, respectively. Estimates of the energy difference (ΔG_{01}) between TS_1 and the bound state were based on the inequality: $\Delta G_{12} + \Delta G_{01} \geq \Delta G^{\circ}$.

Fig. 10 *A* presents the kinetic profiles of the $\alpha_5\beta_1$/FN7-10 interaction. Here, the dissociation rate constant is expressed as a function of pulling force, *f*, according to:

$$k_{off} = 1/\left\{k_1^{\circ -1}\exp[-f\gamma_1/k_BT] + k_2^{\circ -1}\exp[-f\gamma_2/k_BT]\right\},$$

where the subscripts 1 and 2 refer to inner and outer activation energy barriers, respectively (Evans et al., 2001). The kinetic profiles revealed the profound impact of a pulling force on the rate of unbinding of the $\alpha_5\beta_1$/FN7-10 complex (Fig. 10 *A*). As shown, the dissociation rate constant increased exponentially with pulling force from a zero force off rate of ~0.012/s to ~3/s for activated $\alpha_5\beta_1$ at a force of 50 pN. The off rate also increased by about the same amount for low affinity $\alpha_5\beta_1$. The kinetic profiles also revealed that the dissociation rate was less responsive to change in force at higher pulling forces (>~90 pN). It is this ability to resist dissociation at high forces that allowed the $\alpha_5\beta_1$/FN7-10 complex to mediate strong adhesion. It should be noted that the dynamic responses of both low and high affinity forms of the $\alpha_5\beta_1$/FN7-10 interaction are nearly identical at high forces, which would suggest that the molecular determinants of the inner barrier are the same for both high and low affinity $\alpha_5\beta_1$/FN7-10 complexes.

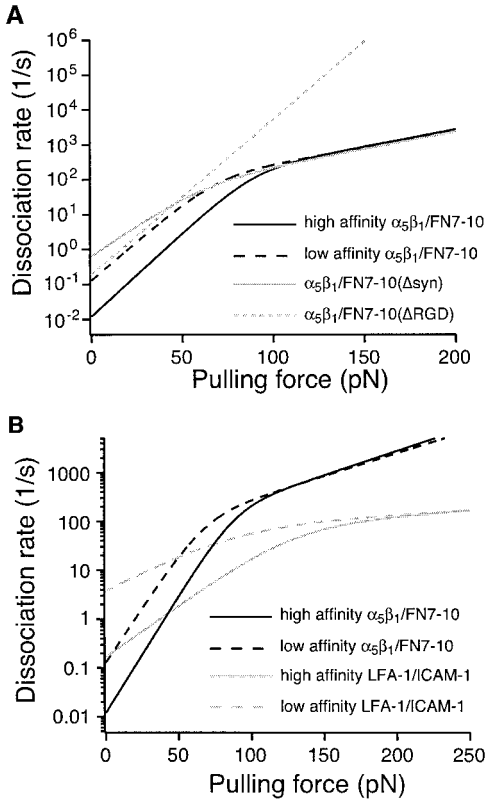

FIGURE 10 Kinetic profiles of the $\alpha_5\beta_1$/FN interaction. (*A*) Effects of FN7-10 mutations on the kinetic profile of the $\alpha_5\beta_1$/FN interaction. (*B*) Comparison of the kinetic profiles of the $\alpha_5\beta_1$/FN7-10 interaction with the LFA-1/ICAM-1 interaction.

Clues into the molecular determinants of the inner and outer activation barriers were derived from the force measurements obtained with site-directed mutants of FN7-10. The RGD loop in domain 10 of FN is crucial for integrin binding. In the $\alpha_V\beta_3$ integrin, the RGD sequence interacts with both the α- and β-subunits (Xiong et al., 2002). The crucial interaction is the electrostatic interaction between the asparate residue of the RGD sequence and the chelated Mg^{2+} ion in MIDAS of the βA domain of the β_1 subunit. Our studies revealed that the deletion of the RGD loop from FN7-10 resulted in the suppression of rupture force of the $\alpha_5\beta_1$/FN complex in the fast loading regime (>10,000 pN/s; Fig. 7). This region of the force spectrum characterizes the inner activation barrier of the complex. Thus, interactions mediated by the RGD sequence appear to be responsible for the inner activation barrier. However, it should be emphasized that deleting the RGD also affected the low force, outer barrier region, where it eliminated the enhanced binding upon integrin activation. Moreover, the frequency of adhesion was substantially reduced for the ΔRGD mutant.

Ligand binding is enhanced by the interactions mediated by synergy site residues in FN9 and the β-propeller of α_5. Our force measurements suggest that the synergy site does not contribute to the inner barrier, but does contribute to the outer barrier of $\alpha_5\beta_1$/FN complex. Just as with the RGD deletion, FN7-10(Δsyn) showed weak binding to unactivated integrin and no enhanced binding upon integrin activation. A further interpretation is that integrin activation involves the outer barrier, which is important in the low force region. At forces of ~5 pN, the force generated by a single myosin or kinesin, the outer barrier, and its regulation by integrin activation is the biologically important feature in the dynamics of adhesion.

It is worthwhile to compare the dynamic response of the $\alpha_5\beta_1$/FN7-10 interaction to other direct force measurements of ligand–receptor interactions. Litvinov et al. (2002) used a laser tweezer apparatus to measure the rupture force of the platelet integrin $\alpha_{IIb}\beta_3$ complexed to its ligand fibrinogen. The reported peak rupture force of 80–100 pN was slightly less than the 120 pN peak that we measured for $\alpha_5\beta_1$/FN at the loading rate of 18,000 pN/s. Interestingly, the authors of this study observed an increase in adhesion frequency upon cell activation by the agonists ADP and thrombin receptor-activating peptide that was attributed to the a change in the accessibility of $\alpha_{IIb}\beta_3$, but observed no change in the rupture force of the integrin/fibrinogen complex upon cell activation. These results are consistent with our findings that both high and low affinity $\alpha_5\beta_1$/FN7-10 complexes exhibited similar rupture forces in the fast loading regime.

Multiple regimes of loading have also been detected in other ligand–receptor systems. In the streptavidin-biotin study, the different loading regimes correlated well with major transitions in the energy landscape of simulated ligand–receptor unbinding (Merkel et al., 1999). Complete force spectra have been obtained for two other binding pairs of adhesion molecules, L-selectin/sLex and LFA-1/ICAM-1, both of which showed a transition to higher slope as loading rates surpassed 10,000 pN/s (Evans et al., 2001; Zhang et al., 2002). Thus, these systems also have inner and outer barriers, which may be common characteristics of all cell adhesion molecules. Moreover, it appears that the inner barrier of these complexes stemmed from electrostatic interaction between a chelated metal cation and a negatively charged amino acid in the binding partner. The adhesion molecule L-selectin binding to its carbohydrate ligand gave a force spectrum with a shape similar to that of $\alpha_5\beta_1$/FN, but with significantly lower forces (Evans et al., 2001). The most frequent rupture forces were 20 and 70 pN at 200 and 20,000 pN/s. In contrast, the adhesion of LFA-1, a leukocyte integrin, binds to its ligand ICAM-1 with higher forces than that of $\alpha_5\beta_1$/FN (Zhang et al., 2002).

A comparison of kinetic profiles of the $\alpha_5\beta_1$/FN7-10 and LFA-1/ICAM-1 complexes revealed that although the $\alpha_5\beta_1$/FN7-10 interaction is more stable than the LFA-1/ICAM-1 interaction with slow dissociation kinetics in the absence of force, the force dependent dissociation of $\alpha_5\beta_1$/FN7-10 interaction is more sensitive to a pulling force. The dissociation rate of the $\alpha_5\beta_1$/FN7-10 complex quickly exceeds the dissociation of the LFA-1/ICAM-1 complex at ~50 pN (Fig. 10 *B*). This analysis shows that the LFA-1/ICAM-1 complex is a more stable adhesion system at force >50 pN and suggests that the $\alpha_5\beta_1$/FN7-10 interaction may not be suited for resisting a large pulling force.

In summary, the current study has identified two barriers to the unbinding of the $\alpha_5\beta_1$/FN complex. An inner barrier, which is affected by deletion of RGD, but not by the synergy site, is seen at high forces that may not be physiologically important. An outer barrier operates at lower, physiologically relevant forces. This outer barrier is affected by both RGD and synergy regions, and it is the site of integrin activation. FN lacking either RGD or synergy site binds weakly to $\alpha_5\beta_1$, and there is no enhancement of binding upon integrin activation. In this low force region $\alpha_5\beta_1$ binding to FN is substantially stronger, with an ~10-fold longer lifetime, than the binding of LFA to ICAM-1.

We thank A. Chen for insightful discussions, C. Freites for technical support, and the reviewers for constructive comments of the original manuscript.

This work was supported by grants from the American Cancer Society and the National Institutes of Health (1 R29 GM55611-01 and R01 CA47056).

REFERENCES

Akiyama, S. K., and S. S. Yamada. 1985. The interaction of plasma fibronectin with fibroblastic cells in suspension. *J. Biol. Chem.* 260:4492–4500.

Aota, S., M. Nomizu, and K. M. Yamada. 1994. The short amino acid sequence Pro-His-Ser-Arg-Asn in human fibronectin enhances cell-adhesive function. *J. Biol. Chem.* 269:24756–24761.

Arroyo, A. G., A. Garcia-Pardo, and F. Sanchez-Madrid. 1993. A high affinity conformational state on VLA integrin heterodimers induced by an anti-beta 1 chain monoclonal antibody. *J. Biol. Chem.* 268:9863–9868.

Aukhil, I., P. Joshi, Y. Yan, and H. P. Erickson. 1993. Cell- and heparin-binding domains of the hexabrachion arm identified by tenascin expression proteins. *J. Biol. Chem.* 268:2542–2553.

Barillari, G., L. Albonici, S. Incerpi, L. Bogetto, G. Pistritto, A. Volpi, B. Ensoli, and V. Manzari. 2001. Inflammatory cytokines stimulate vascular smooth muscle cells locomotion and growth by enhancing alpha5beta1 integrin expression and function. *Atherosclerosis.* 154:377–385.

Bell, G. I., M. Dembo, and P. Bongrand. 1984. Cell adhesion. Competition between nonspecific repulsion and specific bonding. *Biophys. J.* 45: 1051–1064.

Benoit, M., D. Gabriel, G. Gerisch, and H. E. Gaub. 2000. Discrete interactions in cell adhesion measured by single-molecule force spectroscopy. *Nat. Cell Biol.* 2:313–317.

Bowditch, R. D., M. Hariharan, E. F. Tominna, J. W. Smith, K. M. Yamada, E. D. Getzoff, and M. H. Ginsberg. 1994. Identification of a novel integrin binding site in fibronectin. Differential utilization by beta 3 integrins. *J. Biol. Chem.* 269:10856–10863.

Burrows, L., K. Clark, A. P. Mould, and M. J. Humphries. 1999. Fine mapping of inhibitory anti-α5 monoclonal antibody epitopes that differentially affect integrin–ligand binding. *Biochem. J.* 344:527–533.

Caixia, S., S. Stewart, E. Wayner, W. Carter, and J. Wilkins. 1991. Antibodies to different members of the β-1 (CD29) integrins induces homotypic and heterotypic cellular aggregation. *Cell. Immunol.* 138:216–228.

Chen, S., and T. A. Springer. 2001. Selectin receptor-ligand bonds: Formation limited by shear rate and dissociation governed by the Bell model. *Proc. Natl. Acad. Sci. USA.* 98:950–955.

Coe, A. P., J. A. Askari, A. D. Kline, M. K. Robinson, H. Kirby, P. E. Stephens, and M. J. Humphries. 2001. Generation of a minimal α5 β1 integrin-Fc fragment. *J. Biol. Chem.* 276:35854–35866.

Danen, E. H., S. Aota, A. A. van Kraats, K. M. Yamada, D. J. Ruiter, and G. N. van Muijen. 1995. Requirement for the synergy site for cell adhesion to fibronectin depends on the activation state of integrin α5 β1. *J. Biol. Chem.* 270:21612–21618.

Evans, E., and K. Ritchie. 1997. Dynamic strength of molecular adhesion bonds. *Biophys. J.* 72:1541–1555.

Evans, E., K. Ritchie, and R. Merkel. 1995. Sensitive technique to probe molecular adhesion and structural linkages at biological interfaces. *Biophys. J.* 68:2580–2587.

Evans, E., A. Leung, D. Hammer, and S. Simon. 2001. Chemically distinct transition states govern rapid dissociation of single L-selectin bonds under force. *Proc. Natl. Acad. Sci. USA.* 98:3784–3789.

Fernandez, C., K. Clark, L. Burrows, N. R. Schofield, and M. J. Humphries. 1998. Regulation of the extracellular ligand binding activity of integrins. *Front. Biosci.* 3:684–700.

Fritz, J., A. G. Katopodis, F. Kolbinger, and D. Anselmetti. 1998. Force-mediated kinetics of single P-selectin/ligand complexes observed by atomic force microscopy. *Proc. Natl. Acad. Sci. USA.* 95:12283–12288.

Garcia, A. J., F. Huber, and D. Boettiger. 1998a. Force required to break α5β1 integrin–fibronectin bonds in intact adherent cells is sensitive to integrin activation state. *J. Biol. Chem.* 273:10988–10993.

Garcia, A. J., J. Takagi, and D. Boettiger. 1998b. Two-stage activation for α5β1 integrin binding to surface-adsorbed fibronectin. *J. Biol. Chem.* 273:34710–34715.

Garcia, A. J., M. D. Vega, and D. Boettiger. 1999. Modulation of cell proliferation and differentiation through substrate-dependent changes in fibronectin conformation. *Mol. Biol. Cell.* 10:785–798.

George, E. L., E. N. Georges-Labouesse, R. S. Patel-King, H. Rayburn, and R. O. Hynes. 1993. Defects in mesoderm, neural tube and vascular development in mouse embryos lacking fibronectin. *Development.* 119:1079–1091.

Goh, K. L., J. T. Yang, and R. O. Hynes. 1997. Mesodermal defects and cranial neural crest apoptosis in α5 integrin-null embryos. *Development.* 124:4309–4319.

Greiling, D., and R. A. Clark. 1997. Fibronectin provides a conduit for fibroblast transmigration from collagenous stroma into fibrin clot provisional matrix. *J. Cell Sci.* 110:861–870.

Heinz, W. F., and J. H. Hoh. 1999. Spatially resolved force spectroscopy of biological surfaces using the atomic force microscope. *Trends Biotechnol.* 7:143–150.

Hemler, M. E., C. Huang, and L. Schwarz. 1987. The VLA protein family. Characterization of five distinct cell surface heterodimers each with a common 130,000 molecular weight β-subunit. *J. Biol. Chem.* 262:3300–3309.

Hocking, D. C., J. Sottile, and P. J. McKeown-Longo. 1998. Activation of distinct α5β1-mediated signaling pathways by fibronectin's cell adhesion and matrix assembly domains. *J. Cell Biol.* 141:241–253.

Hutter, J. L., and J. Bechhoefer. 1993. Calibration of atomic-force microscope tips. *Rev. Sci. Instrum.* 64:1868–1873.

Hynes, R. O. 1992. Integrins: versatility, modulation, and signaling in cell adhesion. *Cell.* 69:11–25.

Kauf, A. C., S. M. Hough, and R. D. Bowditch. 2001. Recognition of fibronectin by the platelet integrin αIIb β3 involves an extended interface with multiple electrostatic interactions. *Biochemistry.* 40:9159–9166.

Kimizuka, F., Y. Ohdate, Y. Kawase, T. Shimojo, Y. Taguchi, K. Hashino, S. Goto, H. Hashi, I. Kato, K. Sekiguchi, and K. Titani. 1991. Role of type III homology repeats in cell adhesive function within the cell-binding domain of fibronectin. *J. Biol. Chem.* 266:3045–3051.

Litvinov, R. I., H. Shuman, J. S. Bennett, and J. W. Weisel. 2002. Binding strength and activation state of single fibrinogen-integrin pairs on living cells. *Proc. Natl. Acad. Sci. USA.* 99:7426–7431.

Leahy, D. J., I. Aukhil, and H. P. Erickson. 1996. 2.0. A crystal structure of a four-domain segment of human fibronectin encompassing the RGD loop and synergy region. *Cell.* 84:155–164.

Lehenkari, P. P., and M. A. Horton. 1999. Single integrin molecule adhesion forces in intact cells measured by atomic force microscopy. *Biochem. Biophys. Res. Commun.* 259:645–650.

Merkel, R., P. Nassoy, A. Leung, K. Ritchie, and E. Evans. 1999. Energy landscapes of receptor–ligand bonds explored with dynamic force spectroscopy. *Nature.* 397:50–53.

Molla, A., and M. R. Block. 2000. Adherence of human erythroleukemia cells inhibits proliferation without inducing differentiation. *Cell Growth Differ.* 11:83–90.

Mould, A. P., S. K. Akiyama, and M. J. Humphries. 1995. Regulation of integrin α5 β1-fibronectin interactions by divalent cations. Evidence for distinct classes of binding sites for Mn^{2+}, Mg^{2+}, and Ca^{2+}. *J. Biol. Chem.* 270:26270–26277.

Mould, A. P., J. A. Askari, S. Aota, K. M. Yamada, A. Irie, Y. Takada, H. J. Mardon, and M. J. Humphries. 1997. Defining the topology of integrin α5β1-fibronectin interactions using inhibitory anti-α5 and anti-β1 monoclonal antibodies. Evidence that the synergy sequence of fibronectin is recognized by the amino-terminal repeats of the α5 subunit. *J. Biol. Chem.* 272:17283–17292.

Mould, A. P., L. Burrows, and M. J. Humphries. 1998. Identification of amino acid residues that form part of the ligand-binding pocket of integrin α5 β1. *J. Biol. Chem.* 273:25664–25672.

Mould, A. P., J. A. Askari, and M. J. Humphries. 2000. Molecular basis of ligand recognition by integrin α5 β1. I. Specificity of ligand binding is determined by amino acid sequences in the second and third NH2-terminal repeats of the α-subunit. *J. Biol. Chem.* 275:20324–20336.

Moy, V. T., E.-L. Florin, and H. E. Gaub. 1994. Adhesive forces between ligand and receptor measured by AFM. *Colloids Surfaces.* 93: 343–348.

Obara, M., M. S. Kang, and K. M. Yamada. 1988. Site-directed mutagenesis of the cell-binding domain of human fibronectin: separable, synergistic sites mediate adhesive function. *Cell.* 53:649–657.

Oberhauser, A. F., P. E. Marszalek, H. P. Erickson, and J. M. Fernandez. 1998. The molecular elasticity of the extracellular matrix protein tenascin. *Nature.* 393:181–185.

Pierini, L. M., M. A. Lawson, R. J. Eddy, B. Hendey, and F. R. Maxfield. 2000. Oriented endocytic recycling of $\alpha 5\ \beta 1$ in motile neutrophils. *Blood.* 95:2471–2480.

Pierschbacher, M. D., and E. Ruoslahti. 1984. Cell attachment activity of fibronectin can be duplicated by small synthetic fragments of the molecule. *Nature.* 309:30–33.

Redick, S. D., D. L. Settles, G. Briscoe, and H. P. Erickson. 2000. Defining fibronectin's cell adhesion synergy site by site-directed mutagenesis. *J. Cell Biol.* 149:521–527.

Springer, T. A. 1997. Folding of the N-terminal, ligand-binding region of integrin α-subunits into a β-propeller domain. *Proc. Natl. Acad. Sci. USA.* 94:65–72.

Takagi, J., H. P. Erickson, and T. A. Springer. 2001. C-terminal opening mimics 'inside-out' activation of integrin $\alpha 5\beta 1$. *Nat. Struct. Biol.* 8:412–416.

Taverna, D., and R. O. Hynes. 2001. Reduced blood vessel formation and tumor growth in α5-integrin-negative teratocarcinomas and embryoid bodies. *Cancer Res.* 61:5255–5261.

Tees, D. F., R. E. Waugh, and D. A. Hammer. 2001. A microcantilever device to assess the effect of force on the lifetime of selectin–carbohydrate bonds. *Biophys. J.* 80:668–682.

Thoumine, O., P. Kocian, A. Kottelat, and J. J. Meister. 2000. Short-term binding of fibroblasts to fibronectin: optical tweezers experiments and probabilistic analysis. *Eur. Biophys. J.* 29:398–408.

Thoumine, O., and J. J. Meister. 2000. Dynamics of adhesive rupture between fibroblasts and fibronectin: microplate manipulations and deterministic model. *Eur. Biophys. J.* 29:409–419.

Tsuchida, J., S. Ueki, Y. Takada, Y. Saito, and J. Takagi. 1998. The ''ligand-induced conformational change'' of $\alpha 5\ \beta 1$ integrin. Relocation of α5 subunit to uncover the β1 stalk region. *J. Cell Sci.* 111:1759–1766.

Wayner, E. A., S. G. Gil, G. F. Murphy, M. S. Wilke, and W. G. Carter. 1993. Epiligrin, a component of epithelial basement membranes, is an adhesive ligand for $\alpha 3\ \beta 1$ positive T lymphocytes. *J. Cell Biol.* 121:1141–1152.

Xiong, J. P., T. Stehle, B. Diefenbach, R. Zhang, R. Dunker, D. L. Scott, A. Joachimiak, S. L. Goodman, and M. A. Arnaout. 2001. Crystal structure of the extracellular segment of integrin $\alpha V\beta 3$. *Science.* 294:339–345.

Xiong, J. P., T. Stehle, R. Zhang, A. Joachimiak, M. Frech, S. L. Goodman, and M. A. Arnaout. 2002. Crystal structure of the extracellular segment of integrin $\alpha V\beta 3$ in complex with an arg-gly-asp ligand. *Science.* 296:151–155.

Yamada, K. M., and D. W. Kennedy. 1984. Dualistic nature of adhesive protein function: fibronectin and its biologically active peptide fragments can autoinhibit fibronectin function. *J. Cell Biol.* 99:29–36.

Yamada, K. M., and S. Miyamoto. 1995. Integrin transmembrane signaling and cytoskeletal control. *Curr. Opin. Cell Biol.* 7:681–689.

Zhang, X., E. Wojcikiewicz, and V. T. Moy. 2002. Force spectroscopy of the leukocyte function-associated antigen-1 (LFA-1)/intercellular adhesion molecule-1 (ICAM-1) interaction. *Biophys. J.* 83:2270–2279.